Biochemical and Biophysical Research Communications 387 (2009) 169–173

Contents lists available at ScienceDirect

Biochemical and Biophysical Research Communications

journal homepage: www.elsevier.com/locate/ybbrc

The critical iron–oxygen intermediate in human aromatase

Stephanie L. Gantt [a], Ilia G. Denisov [a], Yelena V. Grinkova [a], Stephen G. Sligar [a,b,*]

[a] Department of Biochemistry, University of Illinois at Urbana-Champaign, Urbana, IL 61801, USA
[b] Department of Chemistry, University of Illinois at Urbana-Champaign, Urbana, IL 61801, USA

ARTICLE INFO

Article history:
Received 16 June 2009
Available online 8 July 2009

Keywords:
Cytochrome P450
Aromatase
Peroxo-ferric intermediate
Steroid biosynthesis
EPR (electronic paramagnetic resonance)
Oxy-ferrous heme complex

ABSTRACT

Aromatase (CYP19) is the target of several therapeutics used for breast cancer treatment and catalyzes the three-step conversion of androgens to estrogens, with an unusual C–C cleavage reaction in the third step. To better understand the CYP19 reaction, the oxy-ferrous complex of CYP19 with androstenedione substrate was cryotrapped, characterized by UV–vis spectroscopy, and cryoreduced to generate the next reaction cycle intermediate. EPR analysis revealed that the initial intermediate observed following cryoreduction is the unprotonated $g_1 = 2.254$ peroxo-ferric intermediate, which is stable up to 180 K. Upon gradual cryoannealing, the low-spin ($g_1 = 2.39$) product complex is formed, with no evidence for accumulation of the $g_1 = 2.30$ hydroperoxo-ferric intermediate. The relative stabilization of the peroxo-ferric heme and the lack of observed hydroperoxo-ferric heme distinguish CYP19 from other P450s, suggesting that the proton delivery pathway is more hindered in CYP19 than in most other P450s.

Introduction

Aromatase (CYP19) is a membrane-bound microsomal P450 heme protein that converts androgens to estrogens. This protein is of key medical and pharmaceutical importance, as it is targeted by multiple therapeutic drugs currently used for first-line treatment of estrogen-responsive breast cancer [1]. While CYP19 is found predominantly in the ovaries, testes, and adrenal glands, it is also expressed in the brain, where recent studies suggest that it may play a neuroprotective role [2], further highlighting the importance of understanding CYP19 and the details of its function. For years, biophysical studies have been impeded by the membrane localization of CYP19 and its accompanying tendency to aggregate unless large amounts of detergent were present. To circumvent this problem, we incorporated CYP19 into the native-like membrane environment of Nanodiscs, which stabilizes the protein and allows it to be studied in the absence of detergents [3]. An important advance in our understanding of CYP19 was the recent crystal structure determination [4], providing an atomistic framework for mechanistic understanding.

As a P450 enzyme, CYP19 is thought to proceed through the typical P450 reaction cycle [5]. The reaction begins with substrate binding, which converts the heme iron from 6-coordinate low-spin to 5-coordinate high-spin by displacing a water molecule. The heme iron is then converted from ferric to ferrous by cytochrome P450 reductase (CPR), which acquires reducing equivalents from NADPH. A molecule of dioxygen next binds to the iron, forming the oxy-ferrous complex. This species is reduced by a second electron from CPR, producing the peroxo-ferric intermediate, a nucleophilic species [6]. Two specific protonations ensue, with the first generating the hydroperoxo-ferric intermediate, while the second protonation leads to scission of the O–O bond and the presumed formation of the highly reactive compound I species (Cpd I). Cpd I then generates hydroxylated substrate, which can directly coordinate the heme iron via its hydroxyl group, and subsequently dissociate to allow the next substrate to bind.

Three rounds through this cycle are required for biosynthesis of estrone from AD by CYP19, with the third round potentially deviating from the typical P450 cycle. In the first step, the C19 methyl of AD is hydroxylated, forming 19-hydroxy AD. A second hydroxylation at C19 produces the *gem* diol, which is dehydrated to yield 19-aldo AD. In the third step, which is much more enigmatic, the C10–C19 bond is cleaved, releasing estrone and formate. Two main classes of mechanisms have been proposed for the C–C cleavage step. In one, Cpd I is the key reactive species [7,8]. In the other proposed mechanism, the nucleophilic peroxo-ferric intermediate directly reacts with the substrate's aldehyde functionality, and the resulting peroxo hemiacetal intermediate decomposes to yield the observed products [9].

Chemical precedence for the nucleophilic peroxo-ferric mechanism is given by the non-enzymatic deformylation of a 19-aldo AD mimic by a peroxo-ferric porphyrin model complex [10]. Additionally, evidence suggests that the peroxo-ferric species may be directly used as the reactive intermediate by CYP2B4, CYP17 and CYP51 for C–C cleaving reactions with aldehyde- or ketone-containing substrates, and by nitric oxide synthase [11–14]. However,

* Corresponding author. Address: University of Illinois Urbana-Champaign, 116 Morrill Hall, 505 S. Goodwin Avenue, Urbana, IL 61801, USA. Fax: +1 217 265 4073.
E-mail address: s-sligar@uiuc.edu (S.G. Sligar).

0006-291X/$ - see front matter © 2009 Elsevier Inc. All rights reserved.
doi:10.1016/j.bbrc.2009.06.154

analysis of a minimal CYP19 active site model system by density functional theory found an energetic preference for Cpd I-mediated hydrogen abstraction from the C1 of 19-aldo AD leading to estrone formation, rather than product formation following direct reaction of the peroxo-ferric species with 19-aldo AD [15]. Thus, a clear and consistent picture as to how CYP19 catalyzes the final step in estrone formation and of the relative stability of the intermediate iron-oxygen states, is currently lacking.

The primary distinction between the two mechanisms proposed for the third step in the CYP19 reaction is that in the nucleophilic mechanism, protonation of the peroxo-ferric intermediate is expected to be somewhat impeded, enabling direct reaction of the peroxo-ferric oxygen with the 19-aldo AD substrate. This nucleophilic reaction would be in competition with the protonation of the peroxo-ferric species to subsequently generate Cpd I. To gain insight into the mechanism of CYP19 and the unique features that may equip it for this unique reaction, we sought to trap and characterize the reduced oxygenated intermediates of CYP19. Cryoreduction by γ-irradiation at 77 K is a powerful technique that allows reactive intermediates to be generated and characterized [16–20]. The progression of the cryoreduced intermediate is then monitored during the stepwise increase of temperature (cryoannealing), which allows conformational relaxation and progressively larger motions to occur in the enzyme complex. In wild-type CYP101, the hydroperoxo-ferric intermediate is the first species observed by EPR after cryoreduction at liquid nitrogen temperatures (77 K) [16,19]. The peroxo-ferric intermediate was only observed in CYP101 when the first proton delivery was hindered by mutating Asp251 to asparagine, which allowed us to monitor the conversion of the hydroperoxo-ferric species and finally the product complex as the temperature was increased [19].

To compare the peroxo-ferric intermediate in CYP19 to other P450s, we utilized low temperature oxygenation and subsequent cryoreduction. Surprisingly, we discovered that, in contrast to the other P450 systems, the unprotonated peroxo-ferric intermediate is the predominant species generated by cryoreduction. These are the first observations of the peroxo species in CYP19. Interestingly, when cryoannealed, no hydroperoxo-ferric intermediate is observed, but rather a low-spin product species is directly formed. This end-point complex displayed the same EPR parameters as an authentic ferric 19-hydroxy AD-CYP19 sample. These findings suggest that the proton delivery pathway of CYP19 may be altered relative to that in other P450s, with the important implication for the detailed mechanism of aromatase.

Materials and methods

Expression, purification and self-assembly in Nanodiscs. Modified human CYP19 with a C-terminal His_6-tag and codon usage optimized for *Escherichia coli* (pAr5, based on the pCWori plasmid) was co-expressed in DH5α cells with GroEL/ES chaperones from the commercially available pGro7 plasmid (Takara Bio Inc.) [3,21]. To stabilize CYP19 in a native-like membrane environment, the purified CYP19 was self-assembled into Nanodiscs [3,22,23]. Final concentrations in the disc reconstitution mixture were: 5 mM POPC (Avanti Polar Lipids), 20 mM sodium cholate, 77 μM MSP1D1(−) scaffold protein [24,25], 3.8 μM CYP19, 0.1 M KPi, pH 7.4, 50 mM NaCl, and 5 mM β-ME. After the mixture was incubated on ice for 1 h, an equal volume of moist Amberlite XAD-2 resin (Sigma) was added to the mixture, which was incubated on ice with shaking for 5 h to remove cholate, initiating the self-assembly of CYP19-containing Nanodiscs. Ni–NTA chromatography (Qiagen) was used to remove Nanodiscs lacking the His_6-tagged CYP19. The CYP19-containing Nanodiscs were further purified with a Superdex 200 size-exclusion column (GE Healthcare) to remove any aggregates and CYP19 not incorporated into Nanodiscs. Purified CYP19-containing Nanodiscs (referred to from this point on simply as CYP19) in 0.1 M KPi, pH 7.4, were concentrated. BioUltra grade glycerol (Sigma) was added to a final concentration of 15%, and the protein was flash-frozen in liquid nitrogen and stored at −80 °C.

Trapping and cryoreduction of the CYP19 oxy complex. Concentrated CYP19 with 1 mM AD, methyl viologen (MV:CYP19 ratio of 1:50), 0.1 M KPi, pH 7.4, and 15% glycerol was deoxygenated and reduced with 2.5 M equivalents of dithionite in a Coy Labs anaerobic glove box. The dithionite concentration was determined using its molar absorption coefficient of 8.05 $mM^{-1}\,cm^{-1}$ at 315 nm [26]. To form the oxy-ferrous complex, which was made in triplicate, the reduced CYP19 + AD sample in glycerol was manually injected into a solution of aerobic glycerol-containing buffer precooled to 243 K, mixed for 25 s, transferred to a 200 K dry ice/ethanol bath, and stored in liquid nitrogen. The ferrous-oxy EPR samples were maintained at liquid nitrogen temperatures and cryoreduced by γ-irradiation from a ^{60}Co source as previously described [27] with a dose of 4.5 Mrad [28].

Spectroscopic characterization. All UV–vis absorbance spectra were acquired with a Cary 3 double-beam spectrophotometer (Varian Instruments), using a previously described home-built cryostat cooled with liquid nitrogen for low-temperature absorbance spectra [16,17]. X-Band EPR experiments were performed at the University of Illinois EPR Resource Center on a Varian E-122 X-Band (9.03 GHz) spectrometer, with 0.5 mW microwave power and modulation amplitude of 5 Gauss at 100 kHz. A liquid helium flow system (Air Products) was used to maintain the sample temperature at 15 K.

Results and discussion

Equilibrium species

The addition of AD to CYP19 in Nanodiscs (Materials and methods) induced a spectral shift to high-spin 5-coordinate ferric heme absorbing at 394 nm, indicating fully functional P450 protein [3,29,30]. When saturating amounts of the first reaction cycle product, 19-hydroxy AD, was added to CYP19, only a partial spin shift was seen (Fig. 1), with a larger fraction of low-spin heme than observed for CYP19 + AD [3]. EPR spectra were acquired for ferric CYP19 in the absence of substrate and with AD or 19-hydroxy AD bound. The *g*-values obtained for substrate-free and AD-bound CYP19 were similar to those previously reported for CYP19 in detergent [21], including the observation of two distinct low-spin

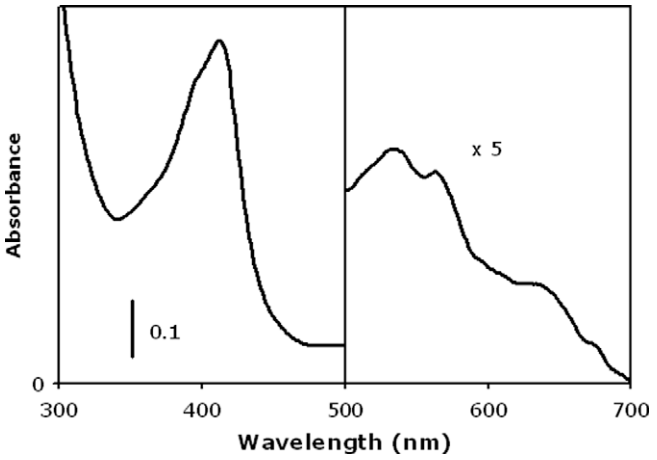

Fig. 1. Optical absorption spectrum of ferric CYP19 + 1 mM 19-hydroxy AD in phosphate buffer.

species for substrate-free CYP19 (Fig. 2). CYP19 + AD was partially high-spin at 15 K, and also had two low-spin species, suggesting some conformational heterogeneity in the initial substrate complex. The EPR spectrum of CYP19 + 19-hydroxy AD acquired at 15 K represented a single low-spin species: $g = [2.39, 2.25, 1.92]$. This is consistent with the higher fraction of low-spin heme observed by UV–vis spectroscopy at 298 K for CP19 + 19-hydroxy AD than for CYP19 + AD (Fig. 1). Notably the g_1 values of substrate-free and 19-hydroxy AD-CYP19 differed slightly, and only CYP19 + 19-hydroxy AD was present as a single species, which should allow substrate-free and product-bound CYP19 to be distinguished by EPR.

Reduction of CYP19

Substrate-free CYP19 was rapidly reduced by addition of dithionite, but reduction was much slower in the presence of AD, requiring tens of minutes for complete reduction. Addition of CO-saturated buffer to ferrous CYP19 + AD results in a CO difference spectrum peak at 448 nm, demonstrating that CYP19 + AD remains in its active P450 form.

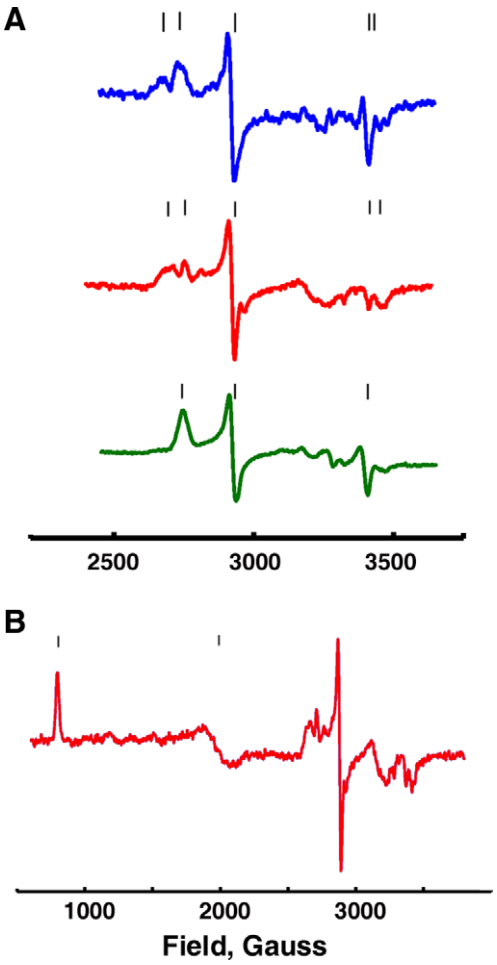

Fig. 2. EPR spectra of ferric CYP19 with no substrate (blue), with androstenedione (AD) (red), and with 19-hydroxy AD (green). (A) Low-spin range with g-values (multiple peaks for the same g-species listed in parentheses): (2.46, 2.41), 2.25, (1.92, 1.90) for substrate-free CYP19; (2.44, 2.39), 2.24, (1.92, 1.90) for CYP19 + AD; and 2.40, 2.245, 1.925 for CYP19 + 19-hydroxy AD. (B) High-spin range with g-values 8.1 and 3.28 for CYP19 + AD. EPR spectra were measured at 15 K, 0.5 mW, and five Gauss modulation at 100 kHz. (For interpretation of color mentioned in this figure the reader is referred to the web version of the article.)

Oxy-ferrous complex of CYP19 + AD

The oxy-ferrous complex of CYP19 + AD was produced by mixing CYP19 + AD with oxygenated glycerol-containing buffer at 243 K and then transferred to 200 K, and stored at 77 K. The absorbance spectrum of the oxy-ferrous CYP19 + AD complex shows the characteristic split hyperporphyrin Soret and Q-band at 555 nm typical of oxy-ferrous intermediates in P450s (Fig. 3) [16], with the same Soret maximum as we previously observed for CYP19 + AD by stopped flow spectroscopy [3].

Peroxo-ferric intermediate

The oxy-ferrous CYP19 + AD sample was cryoreduced at 77 K and the resulting intermediate examined by EPR. The characteristic g_1 values of the peroxo-ferric ($g_1 = 2.25$) and hydroperoxo-ferric ($g_1 = 2.3$) species in P450 enzymes should allow these potential CYP19 intermediates to be distinguished by EPR, while any remaining oxy-ferrous complex is EPR silent [19]. For the CYP19 oxycomplex cryoreduced at 77 K, peaks were seen at $g_1 = 2.254$ and $g_2 = 2.163$ (Fig. 4), with no high-spin ferric iron and no other low-spin species resulting from possible autoxidation of CYP19 during oxygenation. The CYP19 + AD intermediate with $g_1 = 2.254$ is assigned to the peroxo-ferric species, by analogy with the similar peroxo-ferric signal in the D251N, G248T and G248V mutants of CYP101, wild-type CYP101 cryoreduced at 6 K, nitric oxide synthase, peroxidase, hemoglobin and myoglobin [19,31–35] The EPR spectra of Fig. 4 are omitted at 3100 Gauss region, as the organic radicals produced during cryoradiolysis of aqueous glycerol solutions prevent any signals in the neighborhood of $g = 2$ region from being resolved. The signal indicated with a star in the 77 K EPR spectrum of Fig. 4 arises from hydrogen atoms produced during cryoradiolysis [36], and this signal disappears upon annealing at 143 K as the hydrogen radicals recombine. Most striking is our finding that the peroxo-ferric species is the primary CYP19 intermediate observed at 77 K after cryoreduction, which is quite different from other P450s that have been examined by this approach, where the peroxo-ferric species is already protonated at 77 K [19,20].

We gradually annealed the peroxo-ferric CYP19 + AD samples at higher temperatures, with EPR characterization at 15 K after each 2 min cryoannealing step at the indicated temperatures (Fig. 4).

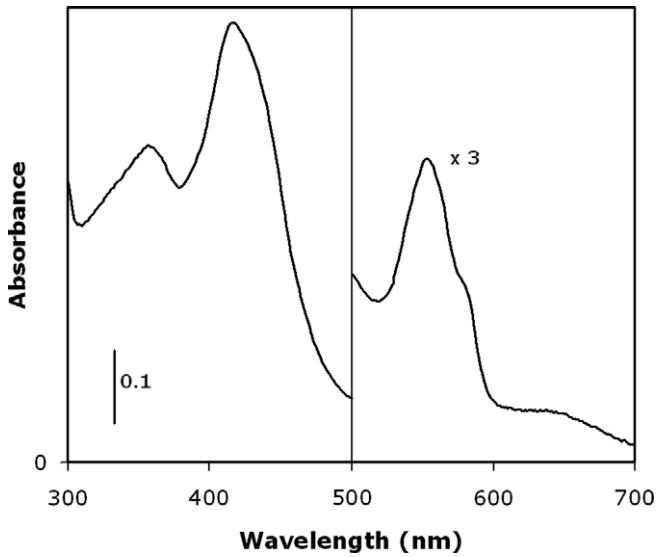

Fig. 3. Optical absorption spectrum of oxy-ferrous intermediate in CYP19 + AD, measured at 130 K in 65% glycerol/ phosphate buffer.

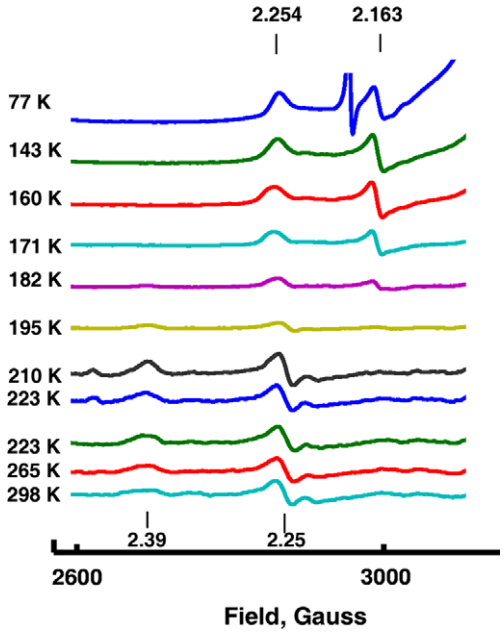

Fig. 4. EPR spectra of peroxo-ferric CYP19 + AD stabilized at 77 K and after sequential annealing for 2 min at indicated temperatures. Peroxo complex with *g*-values 2.254, 2.163 is stable up to 180 K; at 190–220 K this intermediate converts to the product (19-hydroxy AD) complex with *g*-values 2.39, 2.25.

The initial peroxo-anion species was stable from 77 to 180 K. Over the range of 190–220 K, the $g_1 = 2.254$ species converted to $g_1 = 2.39$, with no observable accumulation of the $g_1 = 2.3$ hydroperoxo species. The $g_1 = 2.39$ species is designated as the initial product complex of CYP19 + 19-hydroxy AD, based on the similarity to the equilibrium complex of authentic ferric CYP19 + 19-hydroxy AD ($g_1 = 2.39$) (Fig. 2). Product complexes have previously been observed during the annealing process of the cryoreduced oxy-ferrous complex of camphor-bound CYP101 [19]. Upon further annealing of the CYP19 sample to 298 K, when diffusion becomes possible, the $g_1 = 2.39$ signal diminished, and the predominant feature was the high-spin iron at $g_1 = 8.1$ (data not shown), with less intense low-spin signals at $g_1 = 2.25$ and $g_1 = 2.39$, due to the expected binding of the large excess of AD substrate.

The observation of the peroxo-ferric heme intermediate as the primary species in cryoreduced CYP19, and its direct transition to the $g_1 = 2.39$ product species during cryoannealing suggests fundamental differences in the proton delivery mechanism between CYP19 and other heme proteins such as CYP101, CYP2B4 and heme oxygenase [19,20,34]. An explanation for the difference in proton delivery in CYP19 is that the Asp309 sidechain is oriented quite differently than that of the equivalent Asp251 in CYP101 [4]. This would lead to alterations in the water network, resulting in the active site of CYP19 not being optimized for rapid proton delivery, but rather for stabilizing the peroxo-ferric species so that it could react nucleophilically when an aldehyde-containing substrate is present, such as 19-aldo AD. The stabilization of the peroxo-ferric heme may be a strategy used by multiple heme enzymes, as nitric oxide synthase, which is similarly proposed to use a nucleophilic peroxo-ferric mechanism, and also has a stabilized peroxo-ferric heme species that can be observed at 77 K [12,33].

In summary, in this communication we report for the first time the isolation and characterization of the peroxo-ferric intermediate of CYP19. We propose that the protonation of the CYP19 peroxo-ferric intermediate is hindered, poising it for nucleophilic attack when a suitable aldehyde-containing substrate is present, such as 19-aldo AD. Together, these results provide new insight into the mechanism of this medically important enzyme.

Acknowledgments

We thank M. Rentea and A. Luthra for their technical help, Dr. S. Toshkov for proving access to the ^{60}Co source (Nuclear Radiation Lab, University of Illinois at Urbana-Champaign), and Dr. M. Nilges for help with the EPR spectroscopy. This work was supported by the National Institute of Health Grants GM31756 to S.G. Sligar.

References

[1] C.J. Fabian, The what, why and how of aromatase inhibitors: hormonal agents for treatment and prevention of breast cancer, Int. J. Clin. Pract. 61 (2007) 2051–2063.
[2] C.J. Saldanha, K.A. Duncan, B.J. Walters, Neuroprotective actions of brain aromatase, Front. Neuroendocrinol. 30 (2009) 106–118.
[3] Y.V. Grinkova, I.G. Denisov, M.R. Waterman, M. Arase, N. Kagawa, S.G. Sligar, The ferrous-oxy complex of human aromatase, Biochem. Biophys. Res. Commun. 372 (2008) 379–382.
[4] D. Ghosh, J. Griswold, M. Erman, W. Pangborn, Structural basis for androgen specificity and oestrogen synthesis in human aromatase, Nature 457 (2009) 219–223.
[5] T.M. Makris, R. Davydov, I.G. Denisov, B.M. Hoffman, S.G. Sligar, Mechanistic enzymology of oxygen activation by the cytochromes P450, Drug Metab. Rev. 34 (2002) 691–708.
[6] D.L. Wertz, J.S. Valentine, Nucleophilicity of iron-peroxo porphyrin complexes, Struct. Bond. 97 (2000) 37–60.
[7] K.R. Korzekwa, W.F. Trager, J. Mancewicz, Y. Osawa, Studies on the mechanism of aromatase and other cytochrome-P450 mediated deformylation reactions, J. Steroid Biochem. Mol. Biol. 44 (1993) 367–373.
[8] J. Fishman, M.S. Raju, Mechanism of estrogen biosynthesis. Stereochemistry of C-1 hydrogen elimination in the aromatization of 2 beta-hydroxy-19-oxoandrostenedione, J. Biol. Chem. 256 (1981) 4472–4477.
[9] M. Akhtar, M.R. Calder, D.L. Corina, J.N. Wright, Mechanistic studies on C-19 demethylation in estrogen biosynthesis, Biochem. J. 201 (1982) 569–580.
[10] D.L. Wertz, M.F. Sisemore, M. Selke, J. Driscoll, J.S. Valentine, Mimicking cytochrome P-450 2B4 and aromatase: aromatization of a substrate analogue by a peroxo Fe(III) porphyrin complex, J. Am. Chem. Soc. 120 (1998) 5331–5332.
[11] A.D.N. Vaz, S.J. Pernecky, G.M. Raner, M.J. Coon, Peroxo-iron and oxenoid-iron species as alternative oxygenating agents in cytochrome P450-catalyzed reactions: switching by threonine-302 to alanine mutagenesis of cytochrome P450 2B4, Proc. Natl. Acad. Sci. USA 93 (1996) 4644–4648.
[12] J.J. Woodward, M.M. Chang, N.I. Martin, M.A. Marletta, The second step of the nitric oxide synthase reaction: evidence for ferric-peroxo as the active oxidant, J. Am. Chem. Soc. 131 (2009) 297–305.
[13] A.Z. Shyadehi, D.C. Lamb, S.L. Kelly, D.E. Kelly, W.-H. Schunck, J.N. Wright, D. Corina, M. Akhtar, The mechanism of the acyl-carbon bond cleavage reaction catalyzed by recombinant sterol 14alpha-demethylase of *Candida albicans*, J. Biol. Chem. 271 (1996) 12445–12450.
[14] P. Lee-Robichaud, A.Z. Shyadehi, J.N. Wright, M.E. Akhtar, M. Akhtar, Mechanistic kinship between hydroxylation and desaturation reactions: acyl-carbon bond cleavage promoted by pig and human CYP17 (P-450$_{17\alpha}$; 17α-hydroxylase-17,20-lyase), Biochemistry 34 (1995) 14104–14113.
[15] J.C. Hackett, R.W. Brueggemeier, C.M. Hadad, The final catalytic step of cytochrome P450 aromatase: a density functional theory study, J. Am. Chem. Soc. 127 (2005) 5224–5237.
[16] I.G. Denisov, T.M. Makris, S.G. Sligar, Cryotrapped reaction intermediates of cytochrome P450 studied by radiolytic reduction with phosphorus-32, J. Biol. Chem. 276 (2001) 11648–11652.
[17] I.G. Denisov, T.M. Makris, S.G. Sligar, Cryoradiolysis for the study of P450 reaction intermediates, Methods Enzymol. 357 (2002) 103–115.
[18] I.G. Denisov, S.-C. Hung, K.E. Weiss, M.A. McLean, Y. Shiro, S.-Y. Park, P.M. Champion, S.G. Sligar, Characterization of the oxygenated intermediate of the thermophilic cytochrome P450 CYP119, J. Inorg. Biochem. 87 (2001) 215–226.
[19] R. Davydov, T.M. Makris, V. Kofman, D.E. Werst, S.G. Sligar, B.M. Hoffman, Hydroxylation of camphor by reduced oxy-cytochrome P450cam: mechanistic implications of EPR and ENDOR studies of catalytic intermediates in native and mutant enzymes, J. Am. Chem. Soc. 123 (2001) 1403–1415.
[20] R. Davydov, R. Razeghifard, S.-C. Im, L. Waskell, B.M. Hoffman, Characterization of the microsomal cytochrome P450 2B4 O2 activation intermediates by cryoreduction and electron paramagnetic resonance, Biochemistry 47 (2008) 9661–9666.
[21] N. Kagawa, H. Hori, M.R. Waterman, S. Yoshioka, Characterization of stable human aromatase expressed in *E. coli*, Steroids 69 (2004) 235–243.
[22] T.H. Bayburt, Y.V. Grinkova, S.G. Sligar, Self-assembly of discoidal phospholipid bilayer nanoparticles with membrane scaffold proteins, Nano Lett. 2 (2002) 853–856.
[23] A. Nath, W.M. Atkins, S.G. Sligar, Applications of phospholipid bilayer nanodiscs in the study of membranes and membrane proteins, Biochemistry 46 (2007) 2059–2069.

[24] I.G. Denisov, Y.V. Grinkova, A.A. Lazarides, S.G. Sligar, Directed self-assembly of monodisperse phospholipid bilayer nanodiscs with controlled size, J. Am. Chem. Soc. 126 (2004) 3477–3487.
[25] I.G. Denisov, Y.V. Grinkova, M.A. McLean, S.G. Sligar, The one-electron autoxidation of human cytochrome P450 3A4, J. Biol. Chem. 282 (2007) 26865–26873.
[26] C.E. McKenna, W.G. Gutheil, W. Song, A method for preparing analytically pure sodium dithionite. Dithionite quality and observed nitrogenase-specific activities, Biochim. Biophys. Acta 1075 (1991) 109–117.
[27] I.G. Denisov, P.J. Mak, T.M. Makris, S.G. Sligar, J.R. Kincaid, Resonance Raman characterization of the peroxo and hydroperoxo intermediates in cytochrome P450, J. Phys. Chem. A 112 (2008) 13172–13179.
[28] I.G. Denisov, D.C. Victoria, S.G. Sligar, Cryoradiolytic reduction of heme proteins: maximizing dose dependent yield, Radiat. Phys. Chem. 76 (2007) 714–721.
[29] C.R. Mendelson, E.E. Wright, C.T. Evans, J.C. Porter, E.R. Simpson, Preparation and characterization of polyclonal and monoclonal-antibodies against human aromatase cytochrome-P-450 (P-450arom), and their use in its purification, Arch. Biochem. Biophys. 243 (1985) 480–491.
[30] N. Kagawa, Q.W. Cao, K. Kusano, Expression of human aromatase (CYP19) in *Escherichia coli* by N-terminal replacement and induction of cold stress response, Steroids 68 (2003) 205–209.
[31] Z. Gasyna, Intermediate spin-states in one-electron reduction of oxygen–hemoprotein complexes at low temperature, FEBS Lett. 106 (1979) 213–218.
[32] I.G. Denisov, T.M. Makris, S.G. Sligar, Formation and decay of hydroperoxo-ferric heme complex in horseradish peroxidase studied by cryoradiolysis, J. Biol. Chem. 277 (2002) 42706–42710.
[33] R. Davydov, A. Ledbetter-Rogers, P. Martasek, M. Larukhin, M. Sono, J.H. Dawson, B.S. Siler Masters, B.M. Hoffman, EPR and ENDOR characterization of intermediates in the cryoreduced oxy-nitric oxide synthase heme domain with bound L-arginine or NG-hydroxyarginine, Biochemistry 41 (2002) 10375–10381.
[34] R.M. Davydov, T. Yoshida, M. Ikeda-Saito, B.M. Hoffman, Hydroperoxy-heme oxygenase generated by cryoreduction catalyzes the formation of a-meso-hydroxyheme as detected by EPR and ENDOR, J. Am. Chem. Soc. 121 (1999) 10656–10657.
[35] T.M. Makris, K. von Koenig, I. Schlichting, S.G. Sligar, Alteration of P450 distal pocket solvent leads to impaired proton delivery and changes in heme geometry, Biochemistry 46 (2007) 14129–14140.
[36] J.D. Zimbrick, M.K. Bowman, Concentrated electron scavenger effects on the yields of trapped species in gamma-irradiated alkaline glass, J. Phys. Chem. 76 (1972) 1962–1967.